IEEE Access
Multidisciplinary | Rapid Review | Open Access Journal

Received November 2, 2020, accepted November 12, 2020, date of publication November 17, 2020,
date of current version December 2, 2020.

Digital Object Identifier 10.1109/ACCESS.2020.3038739

3D-Printed Dual-Reflector Antenna With Self-Supported Dielectric Subreflector

ALEJANDRO REBOLLO, ÁLVARO F. VAQUERO, MANUEL ARREBOLA, (Senior Member, IEEE), AND MARCOS R. PINO

Group of Signal Theory and Communications, Department of Electrical Engineering, University of Oviedo, 33202 Gijón, Spain

Corresponding author: Álvaro F. Vaquero (fernandezvalvaro@uniovi.es)

This work was supported in part by the Ministerio de Ciencia, Innovación y Universidades (ARTEINE) under Project TEC2017-86619-R, in part by the European Space Agency under Contract ESTEC/AO/1-7064/12/NL/MH, and in part by the Gobierno del Principado de Asturias/FEDER under Project GRUPIN-IDI/2018/000191.

ABSTRACT A dual-reflector antenna with a self-supported subreflector is proposed. The supporting structure is made of dielectric material and it is part of the feeding of the antenna, which is based on Cassegrain optics and works at X-band. The feeding subsystem includes the primary feed, subreflector supporting structure and subreflector surface in a single dielectric piece, resulting in a compact, light and low-cost solution. First, the subreflector and its feeding subsystem, based on a Dielectric Rectangular Waveguide (DRW) along with a hyperboloid, are described, and the phase center of the DRW and the antenna optics are defined. Then, two effective techniques to mitigate the refraction caused by the dielectric were proposed. Finally, the design was validated through the fabrication of a Cassegrain antenna using a 3D printing technique. Measurements and simulations show a very good agreement and an antenna of 26 dBi of directivity with overall very good performances is obtained, validating both the proposed subreflector and the design technique.

INDEX TERMS Reflector antenna, dual-reflector antenna, 3D printed antennas, aperture antenna, fused filament fabrication, Cassegrain optics.

I. INTRODUCTION

Reflector and dual-reflector antennas are extensively used in applications with high gain requirement such as satellite communications [1], radars [2], or space missions [3], [4]. Due to their geometry, reflector antennas achieve a plane wave at the antenna aperture, obtaining a high gain, low cross-polarization and high efficiency antenna [5]. However, the primary feed in centered configurations is still a problem since the feed has to be placed in the middle of the antenna aperture, causing some blockage in the reflected field and reducing the antenna efficiency. Although this issue is reduced using offset optics, the primary feed needs an auxiliary structure increasing the complexity of the antenna. In addition, a transmission line or waveguide should be used to guide the signal to be radiated to the primary feed, which introduces ohmic losses. As a solution, dual-reflector antennas have been proposed since they typically enhance parameters such as gain or antenna efficiency [5]. In addition, the sidelobe level, the overall ohmic losses and the noise figure are also reduced compared with single reflector antennas [6] because the electronics, such as the receiver, can be placed directly behind the reflector and the antenna feed does not require a long transmission line or waveguide. In this case the blockage is not due to the feed but for the subreflector and the structure needed to sustain it. In order to avoid supporting structures for the subreflector, there has been some research with the aim of obtain a self-supported subreflectors. One of the most common solution in literature is the use of different types of hat-feed [7]–[12], which has proven to be a compact structure to obtain good performances in terms of aperture efficiency [8], [9] because of the corrugations of the metallic hat. However, these corrugations make this solution complex in terms of manufacturing process.

On the other hand, the popularity of 3-D printing techniques to manufacture antennas has increased in recent years because of the cost reduction in the manufacturing process [13]–[15] and the capability to produce complex shapes

The associate editor coordinating the review of this manuscript and approving it for publication was Debdeep Sarkar.

in an easy way, mainly compared with classic 3D milling techniques. These manufacturing techniques have been proposed to be applied to reflector antennas [16], [17], but they are just few works that represent an usual case where only the 3D printing process concerns the reflector, which is later metallized, and they employ standard antennas as primary feeds. The metallization of the reflectors can be achieved through very different techniques, such as [18] vacuum metallization, electroplating or conductive coating. The latter case is faster and more inexpensive that the other two and it is especially suitable when dielectric is the manufacturing material, since it can be applied with aerosol or painting. This metallization technique gives generally good results as it can be observed for instance in [19], where a 3D printed reflector antenna is used in terahertz band and conductive silver spray is used.

In this paper, a dual-reflector antenna with a novel dielectric self-supported subreflector is proposed as an innovative solution exploiting the advantages of 3D printing techniques instead of the traditional use of supporting struts. The proposed subreflector is validated through the design and manufacture of a Cassegrain antenna, discussing the key steps of the designing process. The whole structure is entirely made of dielectric, polylactic acid (PLA), and then conductive spray is used to coat the surfaces of the reflectors. In particular, the feeding subsystem includes the primary feed and the subreflector and it is fabricated in a unique piece. The antenna works in the entire X-band, being validating the designing process through the very good agreement between measured and simulated results. This solution results in a compact, light and inexpensive antenna due to the advantages of 3D-printing techniques.

II. DESCRIPTION OF THE ANTENNA

A. CASSEGRAIN ANTENNA

A Cassegrain antenna is a dual-reflector antenna, which is composed of a main parabolic reflector, a hyperbolic subreflector and a primary feed. In the case of a centered-optics configuration, both the phase center of the feed antenna and the axis of the subreflector are aligned with the axis of the paraboloid, and the structure has axial symmetry. The main section produced by a plane that contents the $z-axis$ of the structure results in a parabola and one branch of a hyperbola, as it is shown in Fig. 1. The reflective surfaces of the paraboloid and the hyperboloid are obtained by the axial rotation of the parabola and hyperbola respectively around the $z-axis$.

Parabola and hyperbola are both conic sections, with one and two foci, respectively. If the phase center of the feeding antenna is placed coincident with one of the foci of the hyperbola, F_1 in Fig. 1, the radiation produced by the feed antenna and reflected by the subreflector would seem to be coming out apparently from the other focus, F_2. Moreover, if the focus of the parabola, F in Fig. 1, is coincident with F_2, the parabola is illuminated by a spherical wavefront with origin in F and therefore it is perfectly focused. Ideally, a plane wave is formed at the antenna aperture and, consequently, a high

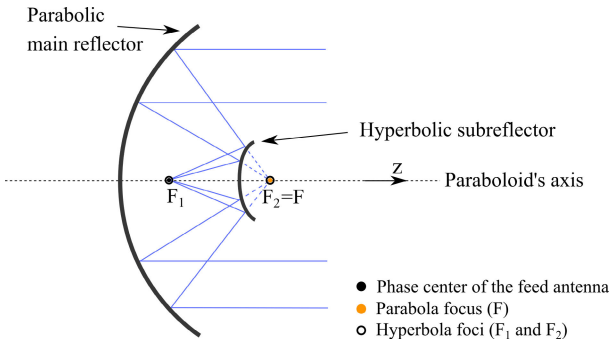

FIGURE 1. Schematic representation of the side view of a Cassegrain antenna, along with the trajectories that four generic rays would follow (in blue).

directivity beam is obtained [5]. However, a structure to hold the subreflector is needed, introducing some blockage for the main reflector.

B. PROPOSED SELF-SUPPORTED SUBREFLECTOR AND FEEDING SUBSYSTEM

Instead of the standard structure, a self-supported subreflector that also includes the feeding system is proposed, obtaining a very compact and one-piece structure as Fig. 2 shows. The feeding system is designed to be fed through a standard rectangular waveguide and a Dielectric Rectangular Waveguide (DRW) with a transition made with a H-plane linear taper [20]. The taper ensures that only the fundamental mode is propagated to the DRW and reduces reflection losses. At the end of the DRW a dielectric cone with modified base is attached. The base of the cone is modified to be a hyperbolic shape instead of flat and is metallized to reflect the incident rays, so it acts as a subreflector of the Cassegrain antenna. The result is a single dielectric piece that includes the feeding and subreflector elements of the antenna and it can be easily joined to the flange of the metallic waveguide.

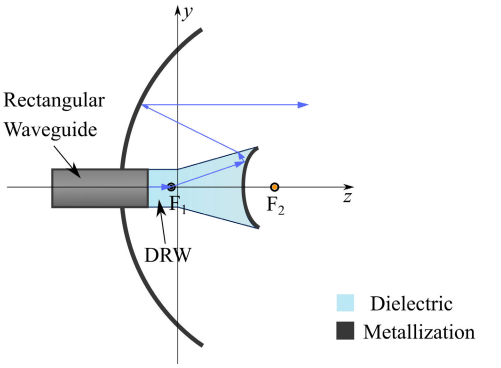

FIGURE 2. Side view of a Cassegrain antenna with a self-supported subreflector, along with the trajectory that one example ray would follow (in blue), using the proposed feeding subsystem.

This concept is valid either for central or offset subreflector configurations, even so for simplicity in this first approach it is applied to central configurations. The geometry of the feed system is detailed in Fig. 3, where the hyperbola centered in

$(0, 0, z_0)$ is defined by

$$\frac{(z-z_0)^2}{a^2} - \frac{y^2}{b^2} = 1 \tag{1}$$

$$a^2 + b^2 = c^2 \tag{2}$$

where a, b and $2c$ are the transverse and conjugate semi-axes and the focal length of the hyperbola, respectively. These parameters fully define the hyperbola shape and, therefore, they are the first to be determined along with the desired radius of the subreflector r_s (see Fig. 3) in order to define the optics. The maximum z value of the delimited hyperbola sets the length L_2 (see Fig 3).

Then, the lines between the ends of the hyperbola and the ends of the DRW define the cone, which it can be seen as the DRW widening, and the value of L_1, which determines the position of the virtual vertex of the cone, is given by (3). Note that h is the diagonal of the section of the DRW.

$$L_1 = L_2 \frac{h/2}{r_s - h/2} \tag{3}$$

The angle α in equation (4) denotes the angle of the generatrix and the axis of the cone, which means the opening of the DRW respect to the $z - axis$, so the size of the feeding subsystem is proportional to it, and it is defined as

$$\alpha = atan\left(\frac{r_s}{L_1 + L_2}\right) \tag{4}$$

Although this approach achieves a relative compact and auto-supported structure, there are some drawbacks that should be in mind. The field reflected by the hyperboloid propagates through two media, dielectric and air, and the medium discontinuity should be taken into account. The outcoming rays towards the subreflector are refracted in the interface air-dielectric, following the Snell's law [21]. Consequently, the reflector is defocused since the foci F_2 of the hyperbola and F of the parabola do not match anymore. As a result, the plane wave at the antenna aperture is not formed properly. Thus, the antenna should be designed in order to ensure that the foci F_1, F_2 and F are accurately placed.

III. DESIGN PROCESS

In this section, the process for the determination of the foci of both the paraboloid and hyperboloid is discussed. Firstly, the procedure consists of setting F_1 by finding the phase center of the DRW, so F_2 can be determined by fixing a focal length of the hyperboloid. Secondly, two different approaches to locate the focus of the paraboloid at F_2 are proposed in order to enhance the focusing of the antenna. One of them involves the focal length of the paraboloid, whereas the other is based on the adjustment of the subreflector geometry.

A. DRW PHASE CENTRE CHARACTERIZATION

If the DRW is attached to a dielectric cone, a spherical wavefront will be generated in this homogeneous medium at the end of the DRW. However, the origin of this spherical wave front may be found in a point, at the DRW, which can be considered the phase center of the feed. Thus, the focus F_1 of the hyperbola (see Fig. 3) must match this point, behaving the phase center as the focal point of the hyperbola. In order to determine its position, an auxiliary elliptical dielectric lens is used. The idea is to connect the DRW with the lens using a dielectric block that ensures a homogeneous propagation medium. When the focus F_1 of the lens is placed at the DRW phase center, a maximum of directivity may be found, since it means perfect collimation and a maximum aperture efficiency [22]. Let us suppose the dielectric structure shown in Fig. 4, which is composed by a DRW, an elliptical dielectric lens and a rectangular block of the same dielectric material. The focus of the lens F_1 is located at $z = 0$. Then, the length block is shorted Δz, thus the lens is displaced, and the focus of the lens is varied along z-axis. Once F_1 is at the phase center of the DRW, a maximum of the directivity is obtained.

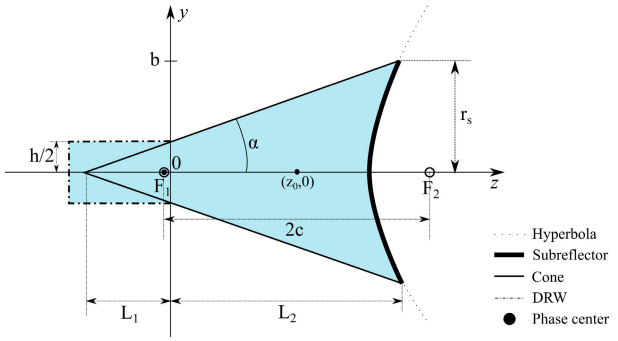

FIGURE 3. Geometric representation of the side view of the proposed feeding subsystem.

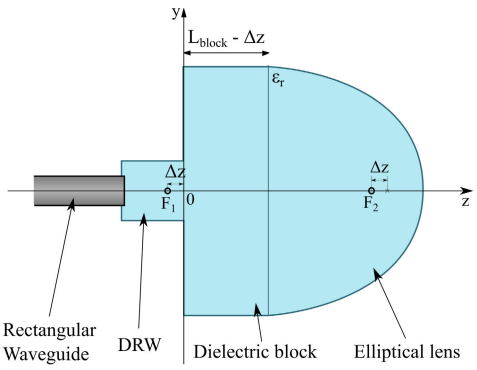

FIGURE 4. Side view of the dielectric structure used to locate the phase center of the DRW.

In order to validate this method, the structure shown in Fig. 4 is simulated in CST Microwave Studio [23], using a dielectric material with $\epsilon_r = 2.75$, and placing the focus F_1 in different positions between 0 and 10 *mm* from the end of the DRW. The focal length [24] of the lens is 98.82 *mm*, the minor and major axes of the ellipse are 50 *mm* and 110.75 *mm*, respectively. The length of the dielectric block $L_{block} - \Delta z$ (see Fig. 4) is 33.76 *mm*, and the length of the DRW is

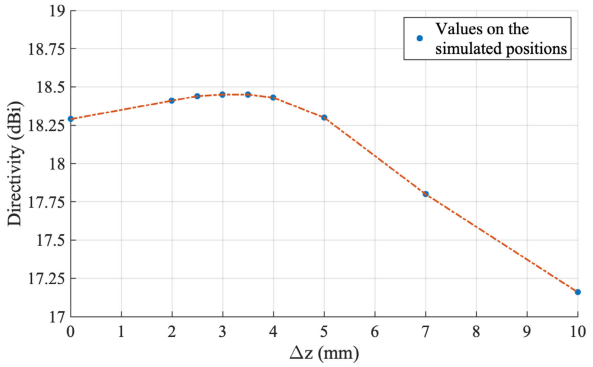

FIGURE 5. Directivity vs penetration of F_1 in the DRW, used to determine the phase center of the primary feed.

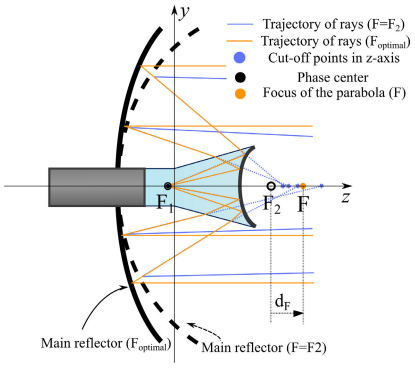

FIGURE 6. Qualitative representation of the solution to the problem of refraction by increasing the focal length of the parabola. In orange, the trajectory of the rays with the new paraboloid, flatter than the previous one. $F_{optimal}$ denotes de position of F where maximum directivity is obtained.

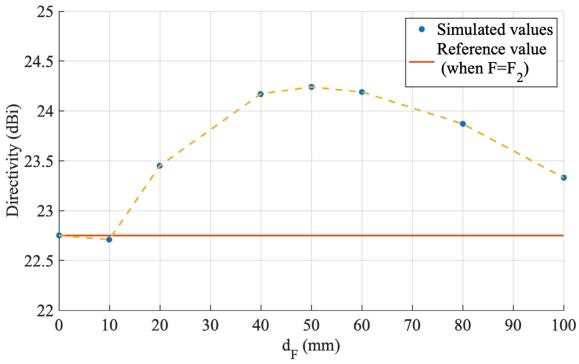

FIGURE 7. Variation of the directivity as a function of the distance between F and F_2, starting from the reference setting ($F = F_2, d_F = 0$).

25 *mm*. The directivity versus Δz is shown in Fig. 5, where a maximum of 18.5 dBi is reached at 3 *mm* from the end of the DRW.

B. INFLUENCE OF THE FOCUS OF THE PARABOLOID

Once the phase center of the DRW is found, it can be used as the focus F_1 of the hyperbolic subreflector. The other parameters of the antenna optics can be then determined considering the second focus of the hyperboloid F_2 and the focus F of the parabolic main reflector, which must match in an ideal case. As it was shown in Fig. 1, in a Cassegrain antenna the rays that go towards the main parabolic reflector once reflected by the hyperboloid surface converge at F_2 due to the properties of the hyperbola. However, in the proposed feed, the rays are refracted in the interface between the dielectric and the air, and the propagation direction changes according to their angle of incidence [24]. Thus, the rays towards the main reflector do not converge at a single point but infinite as Fig. 6 depicts. The main consequence is that a perfect plane wave cannot be obtained at the antenna aperture, including the case of F and F_2 are located at the same point, and additional techniques are needed to minimize this defocusing effect.

One approach is based on increasing the focal length of the paraboloid of the main reflector a value d_F with respect to the case $F = F_2$, as shown in Fig. 6. Although there is not a single converge point, most of the rays converge in a certain area. If the focus of the parabola F is placed at this area, the parabola will be focused properly, and the refraction effect will be reduced. Then, most of the rays will be parallel at the antenna aperture and a plane wave will be nearly obtained.

In order to validate this approach, the directivity of a complete antenna as the one of Fig. 6 was simulated in CST Microwave Studio [23] as a function of d_F, with a hyperboloid with $b = 50$ *mm* and $c = 60$ *mm*, a subreflector with $r_s = 50$ mm, which fixes $L_2 = 103.90$ *mm*, a DRW of 25 *mm* of length, and a parabolic main reflector with 300 *mm* of diameter and 149.50 *mm* of initial focal length. Then, this focal length was increased a value d_F obtaining different values of directivity, as shown in Fig. 7. In this case the area where most of the rays converge is between 40 and 60 *mm* away from F_2, since the difference of directivity due to the election of d_F is negligible there and directivity is maximum in this area. Specifically, the optimal point to place F is 50 *mm* away from F_2, having 1.5 dB more than the case where $F = F_2$. The results probe that placing the focus F in the area where most of the rays converge for every geometry leads to maximizing directivity since the antenna is properly focused.

C. INFLUENCE OF THE GEOMETRY OF THE FEEDING SUBSYSTEM

In previous section it was demonstrated that there is not a single convergence point of the rays but an area due to refraction in the dielectric-air interface, leading to an uncertainty about which is the optimal point to place F since the values in that area are very similar and tend to the maximum. This means that a focus zone is obtained instead a focus point. In this section, the approach is based on reducing the convergence area to reduce the uncertainty and to place it as close as possible to F_2 by controlling the geometry of the cone and subreflector, defining a structure that intrinsically achieves a proper focusing due to the reduction of refraction at the interface dielectric-air.

The angle α (see Fig. 3) defines the tilt of the interface dielectric-air and it has influence in refraction since the deviation depends on the angle of incidence of the outcoming rays from the subreflector by the Snell's law [21]. Applying this law, in a general case without normal incidence with respect to the normal of the interface, situations (a) and (c) in Fig. 8, the rays are refracted having a higher transmitted angle. However, under normal incidence there is no deviation of the rays, see case (b) in Fig. 8.

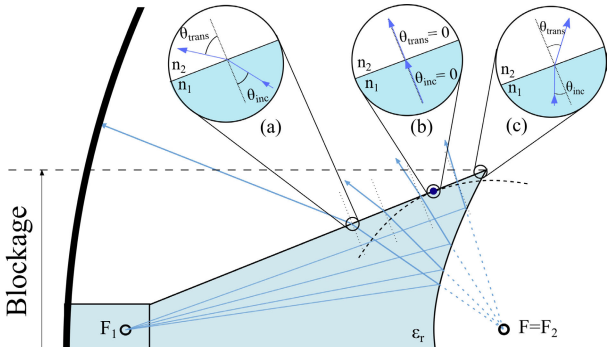

FIGURE 8. Reduction of refraction with an appropriate geometry of the feeding subsystem (enlarged view), with $n_1 > n_2$. The dark blue point denotes the point where the spherical wave front is tangent to the medium discontinuity (normal incidence). Zooms: (a) and (c) Refraction cases; (b) No refraction.

The goal of the method is to make the interface between the dielectric and the air as perpendicular as possible to most of the rays coming from the subreflector, thus finding a balanced solution and minimizing the effect of defocusing because of refraction as represented in Fig. 8. There are parts of the interface that are practically tangent to the spherical wavefront with origin in F_2, so that angles of incidence of the rays are close to be normal to the interface, being most of the rays properly focused in that case. Note that in the case of deviation, the rays may be directed towards the reflector, increasing the blockage of the subreflector as in case (a), or in the opposite angle, increasing the spillover as in case (c).

Specifically, normal incidence is achieved in the point of tangency between the cone and the spherical wavefront with F_2 as origin, and this point depends mainly on the eccentricity of the hyperbola, the radius of the subreflector r_s (see Fig. 3) and the longitudinal length of the feeding subsystem $L_1 + L_2$ (see Fig. 3), giving an angle α which has to minimize refraction. If this point is placed very close to the edge of the subreflector, all rays will be practically curved to the reflector by refraction. If it is placed close to the point where rays are blocked, most of them will be directed outside the main parabolic reflector. Because of that, there will be an area of the cone where fixing the point of tangency to make the interface close to the circumference, mitigating the effect of refraction and achieving higher directivity values.

In order to validate the method three geometries of the feeding subsystem were analyzed, all of them having the same eccentricity. The parameters of the geometries are

TABLE 1. Parameters of the compared subreflector geometries.

Parameter	Geometry 1	Geometry 2	Geometry 3
b (mm)	50.0	30.0	20.0
c (mm)	60.0	36.0	24.0
r_s (mm)	50.0	45.0	40.0
L_1 (mm)	38.1	29.3	25.6
L_2 (mm)	103.9	68.9	50.7
α (°)	19.4	24.6	27.7

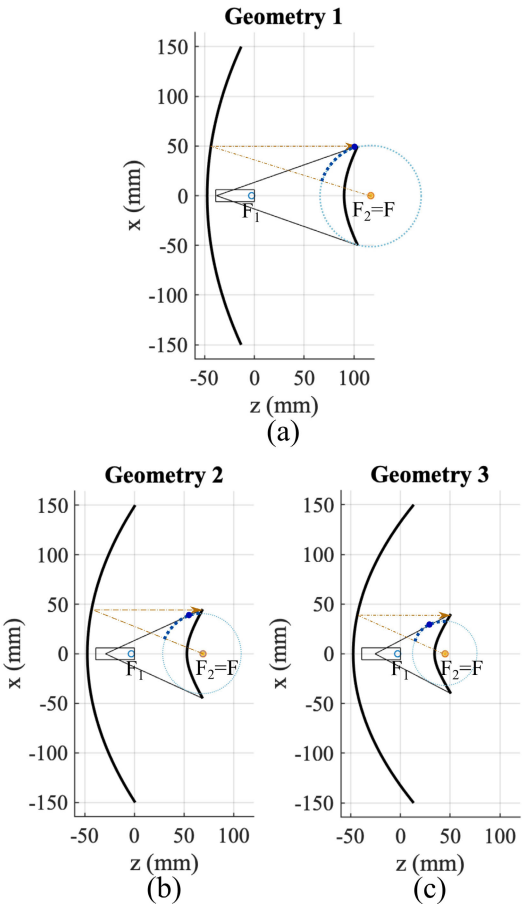

FIGURE 9. Side view of the analyzed subreflector geometries, where F_1 and F_2 are the foci of the hyperbola and F is the focus of the parabola. The orange line denotes the first ray that suffers blockage from the subreflector, the dark blue point denotes the tangency point, and the dashed blue circumference denotes the spherical wave with origin in F_2, where the dark blue dotted arc denotes the effective portion of it where rays do not suffer blockage. (a) Geometry 1, (b) Geometry 2 and (c) Geometry 3.

detailed in Table 1. The main difference between them is that the distance between foci of hyperbola was gradually decreased. As a consequence, the radius r_s was also decreased to reduce the blockage produce by the subreflector and giving higher angles α in this case.

As shown in Fig 9, a parabolic main reflector of 300 *mm* of diameter was added to simulate Geometries 1, 2 and 3 in CST Microwave Studio [23], with a focal length of

149.5 *mm*, 115.5 *mm* and 91.5 *mm*, respectively. It also has been represented the arc of circumference that represents normal incidence in the effective surface of the cone, the part where the rays do not suffer blockage from the subreflector. The results of gain are summarized in Table 2. In this case, higher gain is obtained with Geometries 2 and 3 than with Geometry 1. As shown in Fig 9, the tangency point is nearly to the edge of the subreflector in Geometry 1, and the interface dielectric-air is far from being normal to the rays. In the case of Geometries 2 and 3 their points are more in the middle of the effective area making the interface very close to the circumference, achieving very low incidence angles at most of its surface. Note that different points of tangency give similar results, and the increase in directivity due to the refraction is less significative than in Geometry 1. These results validate the proposed method as a principle of design of the proposed antenna to find an optimal geometry of feeding subsystem and subreflector.

TABLE 2. Gain (dB) of the simulated subreflector geometries using CST.

Parameter	Geometry 1	Geometry 2	Geometry 3
Gain (dB)	16.90	22.54	22.08

IV. EXPERIMENTAL VALIDATION

A. ANTENNA OPTICS

In order to validate the techniques a dual-reflector antenna at 10 GHz is manufactured using a 3D printing technique. The used DRW has a rectangular section of dimension 12 *mm* × 24 *mm* and a length of 39 *mm*, and the transition to the WR-90 that feeds the system is done by a linear H-plane taper.

The design was carried out to minimize the effect of refraction by making the interface dielectric-air as perpendicular as possible to the rays. The best geometry of those analyzed, in terms of gain, is Geometry 2 from Table 1. The value of the diameter of the main reflector was fixed at 300 mm (10λ at working frequency), and the focal length of the paraboloid, 115.5 mm, is such that F=F_2, being in this case negligible the improvement obtained displacing F.

B. PRIMARY FEED CHARACTERIZATION

The structure composed of the DRW and the cone acts as the primary feed of the antenna propagating the wave towards the subreflector. The structure is measured and simulated in a full-wave simulation in order to study its performances. In Fig. 10 the return losses both measured and simulated are compared in the whole X-band, from 8 to 12 GHz. In a first approach, the PLA dielectric constant was estimated to 2.75 [25], even so the simulated S_{11} shows a shift regarding the measured S_{11}. After a slight variation in the PLA permittivity from 2.75 to 2.65, a highly agreement between measurements and simulations is found and shows a good match of the structure, mainly due to the linear H-plane

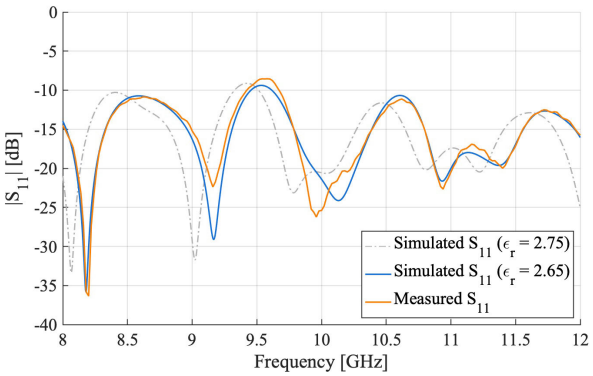

FIGURE 10. Comparison of the return losses measured and simulated of the proposed feeding system.

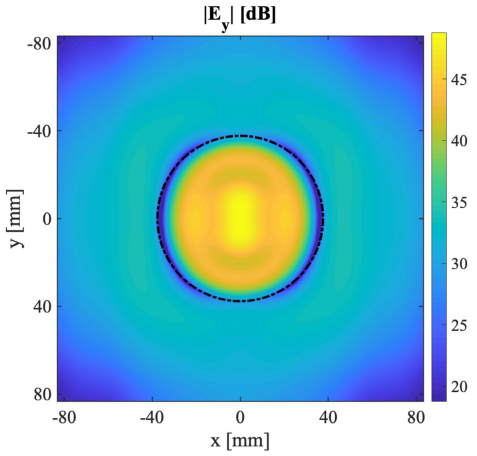

FIGURE 11. Copolar electric field at the subreflector plane at z=52.9 mm, showing the illumination shape and the spillover.

taper. Hereinafter, the dielectric constant of the PLA is set to 2.65. The electric field distribution on a plane in front of the subreflector is shown in Fig. 11 and the main planes in Fig. 12. The spillover efficiency of the subreflector is estimated in a 73.76% (1.32 dB loss), according to Fig. 12, while the taper on the subreflector surface is not symmetrical regarding its main planes, and a taper of −15 dB is found in $\varphi = 0°$ and $\varphi = 90°$, for subtended half-angles of $\theta = 23.5°$ and $\theta = 21.5°$ respectively.

C. FABRICATION

The antenna geometry given by the parameters of the previous section was manufactured using *Fused Filament Fabrication*, a 3D-printing technique based on depositing stacked layers of a thermoplastic material trough a mobile extruder to conform the piece. The dielectric used was polylactic acid (PLA), a thermoplastic with $\epsilon_r = 2.75$ and $\tan\delta = 0.015@60GHz$ [25]. The prototype was printed using an Ultimaker 3, which its maximum printing volume led to slice the main reflector into 6 pieces in order to make feasible printing it, whereas the feeding subsystem remained in one PLA piece, as shown in Fig. 13. The pieces were printed in

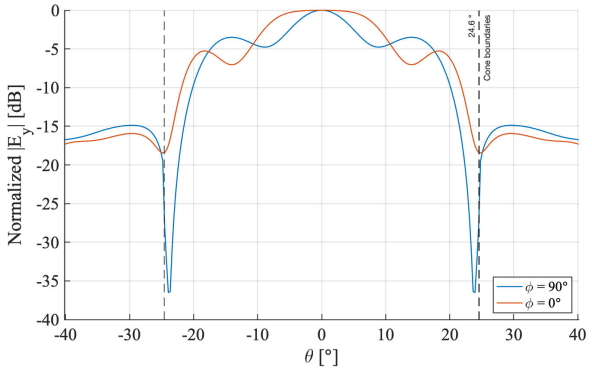

FIGURE 12. Main planes of the simulated E-field distribution of the primary feed in a plane at z=52.9 mm, which is the plane at the subreflector aperture.

PLA with a precision of 0.2 *mm*, enough since the wavelength at 10 GHz is much larger and small imperfection on the reflector surfaces intrinsic to the manufacturing process do not affect the performance [19].

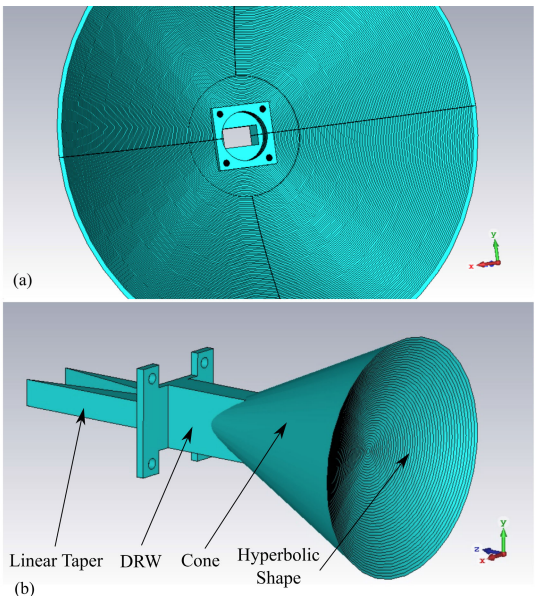

FIGURE 13. Final antenna design: (a) Main Reflector (b) Feeding subsystem (Taper, DRW, Cone and Hyperbolic Shape).

Once the pieces were manufactured and assembled, the reflector parabolic and subreflector hyperbolic dielectric surfaces were metallized. The metallization was applied using a conductive metal spray (841AR from MG Chemicals) to coat uniformly those surfaces. The final dual reflector is shown in Fig. 14.

D. MEASUREMENTS

The manufactured dual-reflector antenna was evaluated in the anechoic chamber at the University of Oviedo. The setup consists of the dual-reflector and a standard pyramidal horn antenna of 20 dBi gain as probe, both connected to the ports of a vector network analyzer R&S©ZVK of Rohde&Schwarz.

FIGURE 14. 3D-printed dual-reflector antenna with the proposed subreflector in the measurement chamber.

The field was evaluated in a spherical range at several frequencies between 8 and 12 GHz, covering the whole X-band.

Because of the dimensions of the antenna under test and measurement facility, the acquisition is carried out in near-field (NF) and transformed to far-field (FF) with a near-field to far-field (NF-FF) transformation. The two spherical components of the electric field (E_θ and E_ϕ) are measured in a 3-D acquisition. Then, the SNIFT from TICRA [26] is used to carried out the NF-FF transformation based on Spherical Wave Expansion (SWE). The resulting radiation pattern at 10 GHz is shown in Fig. 15. The peak directivity is 26.1 dBi and the maximum value of cross-polar, which is in the $\phi = 45°$ plane, is 6 dBi, resulting in 20 dB of CP/XP ratio, and the side lobe level is around 12 dB. The measured gain of the antenna is 24 dBi, and the difference with the original simulated value (23.11 dBi) is due to overestimate the losses of PLA, since the antenna has been also simulated considering lossless materials and 26.28 dBi gain has been obtained. The efficiencies of the antenna have been computed, obtaining 70.41% spillover efficiency (1.52 dB loss) and 61.63% blockage efficiency (2.10 dB loss). In the case of the equivalent ideal Cassegrain antenna, the cumulative loss gain because of aperture efficiency is in the order of 2.8 dB, [27]. The prototype was thoughtfully aligned using a laser, consequently the main beam is in the direction (0,0) and good symmetry is obtained about the boresight axis. This symmetry can also be observed at Fig. 16, where measured and simulated co-polar normalized radiation patterns of the antenna at 10 GHz in the $\phi = 0°$ and $\phi = 90°$ planes are compared, along with the cut where maximum cross-polar, $\phi = 45°$. Very good agreement between simulations and measurements is obtained, validating the manufactured antenna and the proposed self-supporting subreflector model.

Moreover, the variation of the radiation patterns in the X-band is shown in Fig. 17, from 8 to 12 GHz, which

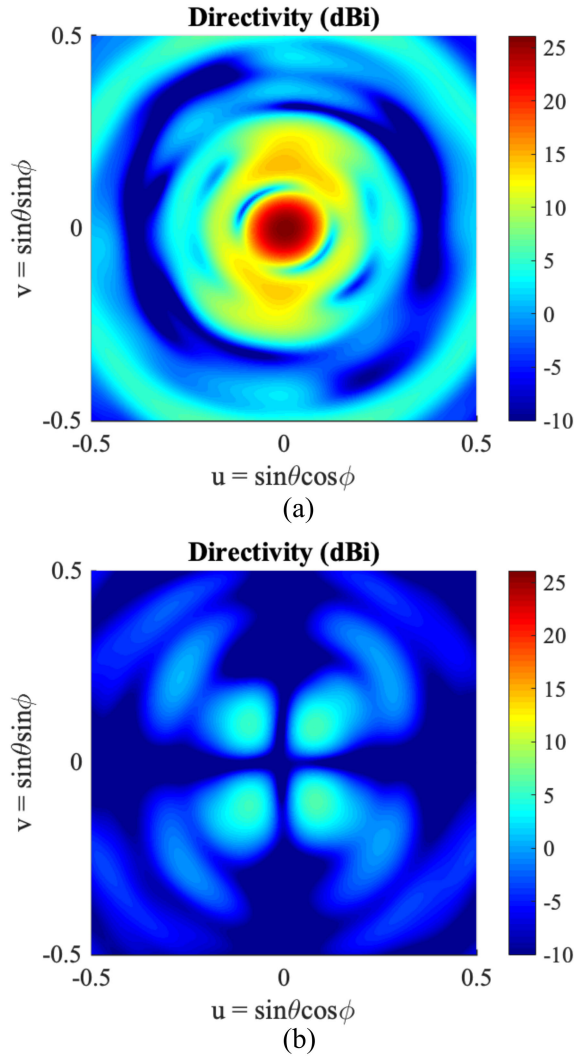

FIGURE 15. Measured radiation pattern at 10 GHz at (a) Co-polar and (b) Cross-polar.

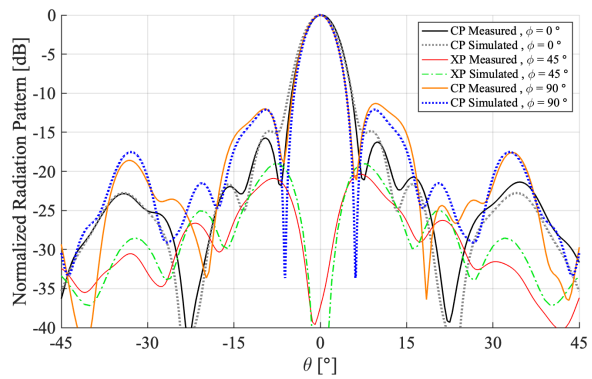

FIGURE 16. Measured and simulated radiation patterns in the main planes, where $\phi = 0°$ (H-Plane) and $\phi = 90°$ (E-Plane).

corresponds with the recommended use bandwidth of a WR-90 waveguide. Although the maximum directivity is slightly lower for frequencies below 10 GHz (design frequency) because for those frequencies the main reflector

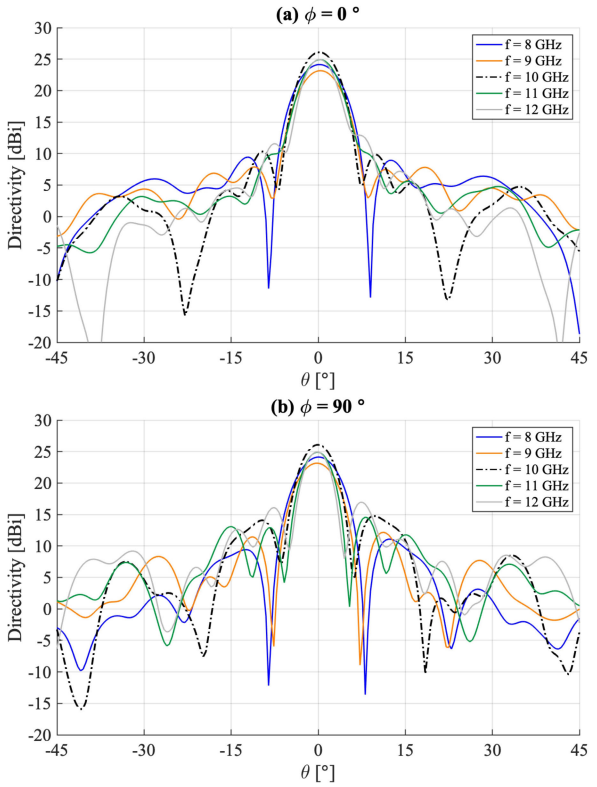

FIGURE 17. Measured co-polar radiation patterns across the X-band in the main planes. (a) $\phi = 0°$ (H-Plane) and (b) $\phi = 90°$ (E-Plane).

TABLE 3. Quantitative comparative analysis of the proposed antenna with the state of the art of antennas with self-supported subreflector at X-band.

Parameter	Compact Wideband Hat-Feed [8]	Hat-Feed without dielectric [9]	Proposed antenna
Center frequency (GHz)	12.625	11.5	10
Material	Metal and dielectric	Metal	Dielectric (PLA)
Diameter of main reflector	22.3λ	25.1λ	10λ
Gain (dB)	35 @12.75 GHz	35 @11.5 GHz	24 @10 GHz
Aperture efficiency (%)	60.3 @12.75 GHz	53.1 @11.5 GHz	66.8 @10 GHz
Fractional BW (%)	30	26	40

is electrically smaller, the difference is 2.9 dB or less, resulting in a broadband solution with fractional bandwidth larger than 40%. Therefore, the antenna is focused on the whole band and the major limitation in the bandwidth is the monomode operational bandwidth of the WR-90 waveguide used as primary feed.

Only few published works may be found about self-supported structures as subreflector in reflector antennas and one common approach in literature to obtain one of these compact structures is the waveguide hat-feed, which is based

on metallic corrugations. Two of these models have been chosen to make a comparison with the proposed antenna as they are also fed by waveguide and their operating frequency is in X-band, and the result is shown in Table 3. Specifically, in [8] a metallic hat-feed with dielectric head is proposed and it is tested along with a parabolic reflector, presented as a solution to achieve high values of phase efficiency. In [9], a novel type of hat-feed is proposed using only metal as material. As shown in Table 3, the proposed antenna exhibits lower directivity than both hat-feed models, but this is due to the use of dielectric as propagating material in the feed and the use of much smaller subreflector. On the contrary, it achieves higher aperture efficiency values, computed as the product of spillover and illumination efficiencies, and larger bandwidth, providing a better broadband solution than the analyzed models.

V. CONCLUSIONS

A Cassegrain antenna with novel dielectric self-supported subreflector is proposed in this paper as a low cost and effective solution. The structure is based on a cone ended in a hyperboloid shape attached to a DRW and it is fully made of dielectric, resulting in a compact, light and low-cost technological solution. With a hyperboloid defined, the design essentially comprises the location the phase center of the DRW and foci of the hyperbola. Refraction may be caused using dielectric, but two different design techniques are proposed in order to mitigate its effect. Both proved effective, one is based on increasing the focal length of the main reflector and the other one is based on a suitable design of the subreflector. Specifically, the proper election of the distance between foci, the eccentricity, and the radius of the subreflector can achieve lower defocusing and higher gain. A Cassegrain antenna was manufactured using a 3D printing technique and PLA as dielectric in order to validate the proposed subreflector at 10 GHz. Conductive metal spray was used to make the metallization of the reflector surfaces. There is very good agreement between simulations and measurements, obtaining an antenna with 24 dBi gain and low-level sidelobes, good behavior in the frequency band and a CP/XP ratio of 20 dB, which demonstrates the good performance of the subreflector. Additionally, these results validate the proposed designing technique, which may be extended to millimeter frequencies in future developments.

REFERENCES

[1] T. Takahashi, "Disaster satellite communication experiments using WINDS and wireless mesh network," in *Proc. 16th Int. Symp. Wireless Pers. Multimedia Commun. (WPMC)*, Atlantic City, NJ, USA, 2013, pp. 1–4.

[2] S. Futatsumori, K. Morioka, A. Kohmura, and N. Yonemoto, "Design and measurement of W-band offset stepped parabolic reflector antennas for airport surface foreign object debris detection radar systems," in *Proc. Int. Workshop Antenna Technol., Small Antennas, Novel EM Struct. Mater., Appl.*, Sydney, NSW, Australia, Mar. 2014, pp. 51–52.

[3] Z. A. Pour and L. Shafai, "A simplified feed model for investigating the cross polarization reduction in circular- and elliptical-rim offset reflector antennas," *IEEE Trans. Antennas Propag.*, vol. 60, no. 3, pp. 1261–1268, Mar. 2012.

[4] N. N. Gorobets, V. I. Kiyko, and V. N. Gorobets, "Dependence of the lateral and cross-polarized radiation reflector antennas on their size and focal length," in *Proc. Int. Conf. Antenna Theory Techn.*, Odessa, Japan, Sep. 2013, pp. 434–437.

[5] S. J. Orfanidis, "21. Aperture Antennas," in *Proc. Electron. Waves Antennas*, Piscataway, NJ, USA, 2016, pp. 1065–1085. [Online]. Available: www.ece.rutgers.edu/ orfanidi/ewa

[6] P. Hannan, "Microwave antennas derived from the cassegrain telescope," *IRE Trans. Antennas Propag.*, vol. 9, no. 2, pp. 140–153, Mar. 1961.

[7] P.-S. Kildal, "The hat feed: A dual-mode rear-radiating waveguide antenna having low cross polarization," *IEEE Trans. Antennas Propag.*, vol. 35, no. 9, pp. 1010–1016, Sep. 1987.

[8] E. G. Geterud, J. Yang, T. Ostling, and P. Bergmark, "Design and optimization of a compact wideband hat-fed reflector antenna for satellite communications," *IEEE Trans. Antennas Propag.*, vol. 61, no. 1, pp. 125–133, Jan. 2013.

[9] W. Wei, J. Yang, T. Ostling, and T. Schafer, "New hat feed for reflector antennas realised without dielectrics for reducing manufacturing cost and improving reflection coefficient," *IET Microwaves, Antennas Propag.*, vol. 5, no. 7, pp. 837–843, May 2011.

[10] F. Greco, G. Amendola, L. Boccia, and E. Arnieri, "A dual band hat feed for reflector antennas in Q-V band," in *Proc. 10th Eur. Conf. Antennas Propag. (EuCAP)*, Davos, Switzerland, Apr. 2016, pp. 1–4.

[11] Y.-J. Zhao, B.-C. Zhu, Y.-B. Meng, and Z.-H. Yan, "Design of a hat feed for ring focus reflector antenna," in *Proc. Int. Conf. Microw. Millim. Wave Technol. (ICMMT)*, Guangzhou, China, May 2019, pp. 1–3.

[12] M. Yousefnia, A. Pirhadi, and M. Hakkak, "Analysis and design of parabolic hat feed antenna," in *Proc. IEEE Antennas Propag. Soc. Int. Symp.*, Washington, DC, USA, 2005, pp. 650–653, doi: 10.1109/APS.2005.1552337.

[13] M. Liang, J. Wu, X. Yu, and H. Xin, "3D printing technology for RF and THz antennas," in *Proc. Int. Symp. Antennas Propag. (ISAP)*, Okinawa, Haryana, 2016, pp. 536–537.

[14] S. K. Sharma, "Impact of inkjet and 3D printing methods on low weight and complex structure antennas," in *Proc. 18th Int. Symp. Antenna Technol. Appl. Electromagn. (ANTEM)*, Waterloo, ON, USA, Aug. 2018, pp. 1–2.

[15] M. van der Vorst and J. Gumpinger, "Applicability of 3D printing techniques for compact ku-band medium/high-gain antennas," in *Proc. 10th Eur. Conf. Antennas Propag. (EuCAP)*, Davos, Switzerland, Apr. 2016, pp. 1–4.

[16] L. G. Menéndez, O. S. Kim, F. Persson, M. Nielsen, and O. Breinbjerg, "3D printed 20/30-GHz dual-band offset stepped-reflector antenna," in *Proc. 9th Eur. Conf. Antennas Propag. (EuCAP)*, Lisbon, Portugal, 2015, pp. 1–2.

[17] J. Romeu, S. Blanch, N. Vidal, J. M. Lopez-Villegas, and A. Aguasca, "Assessment of 3-D printing technologies for millimeter-wave reflectors," *IEEE Antennas Wireless Propag. Lett.*, vol. 17, no. 11, pp. 2061–2064, Nov. 2018.

[18] K. V. Hoel, S. Kristoffersen, J. Moen, K. G. Kjelgard, and T. S. Lande, "Broadband antenna design using different 3D printing technologies and metallization processes," in *Proc. 10th Eur. Conf. Antennas Propag. (EuCAP)*, Davos, Switzerland, Apr. 2016, pp. 1–5.

[19] S. Adibelli, P. Juyal, C.-L. Cheng, and A. Zajic, "Terahertz near-field focusing using a 3-D printed cassegrain configuration for backscattered side-channel detection," *IEEE Trans. Antennas Propag.*, vol. 67, no. 10, pp. 6627–6638, Oct. 2019.

[20] S. Dudorov, "Rectangular dielectric waveguide and its optimal transition to a metal waveguide," Ph.D. dissertation, Dept. Elect. Commun. Eng., Helsinki Univ. Technol., Espoo, Finland, Jun. 2002.

[21] D. M. Pozar, *Microwave Engineering*, 4th ed. Hoboken, NJ, USA: Wiley, 2011.

[22] J. R. Costa, E. B. Lima, and C. A. Fernandes, "Antenna phase center determination from amplitude measurements using a focusing lens," in *Proc. IEEE Antennas Propag. Soc. Int. Symp.*, Toronto, ON, Canada, Jul. 2010, pp. 1–4.

[23] CST Microwave Studio. (Jul. 2020). *Computer Simulation Technology*. [Online]. Available: http://www.cst.com

[24] C. A. Fernandes, E. B. Lima, and J. R. Costa, "Dielectric Lens Antennas," in *Handbook of Antenna Technologies*, Z. Chen, D. Liu, H. Nakano, X. Qing, and T. Zwick, Eds. Singapore: Springer, 2016.

[25] J. M. Felicio, C. A. Fernandes, and J. R. Costa, "Complex permittivity and anisotropy measurement of 3D-printed PLA at microwaves and millimeter-waves," in *Proc. 22nd Int. Conf. Appl. Electromagn. Commun. (ICECOM)*, Dubrovnik, Croatia, Sep. 2016, pp. 1–6.
[26] *GRASP V10*, TICRA, Copenhagen, Denmark, 2016.
[27] P.-S. Kildal, *Foundations of Antenna Engineering A Unified Approach for Line-of Sight and Multipath*. Norwood, MA, USA: Artech House, 2015.

ALEJANDRO REBOLLO was born in León, Spain, in 1997. He received the B.Sc. degree in telecommunications engineering from the University of Oviedo, Oviedo, Spain, in 2019, where he is currently pursuing the M.Sc. degree.

Since 2019, he has been a Research Assistant with the Signal Theory and Communications Area, University of Oviedo, being involved in a project with the European Space Agency. His current research interests include the design of 3-D-printed antennas, such as dual-reflectors and antennas at mm-wave frequencies.

ÁLVARO F. VAQUERO was born in Salinas, Spain, in 1990. He received the B.Sc. and M.Sc. degrees in telecommunications engineering from the Universidad de Oviedo at Gijón, Gijón, Spain, in 2015 and 2017, respectively, where he is currently pursuing the Ph.D. degree.

Since 2016, he has been a Research Assistant with the Signal Theory and Communications Area, University of Oviedo. In 2017, he was with the Instituto de Telecomunicações, Lisbon, Portugal, where he was involved in broadband planar lenses for skin cancer imaging. His current research interests include the development of efficient techniques for the analysis and synthesis of planar antennas, especially reflectarray and transmitarrays and the design of 3-D printed lenses for near-field applications.

MANUEL ARREBOLA (Senior Member, IEEE) was born in Lucena, Córdoba, Spain. He received the M.Sc. degree in telecommunication engineering from the University of Málaga, Málaga, Spain, in 2002, and the Ph.D. degree from the Technical University of Madrid (UPM), Madrid, Spain, in 2008.

From 2003 to 2007, he was a Research Assistant with the Department of Electromagnetism and Circuit Theory, UPM. In 2005, he was a Visiting Scholar with the Department of Microwave Techniques, Universität Ulm, Ulm, Germany. In 2007, he joined the Department of Electrical Engineering, University of Oviedo at Gijón, Gijón, Spain, where he is currently an Associate Professor. In 2009, he was with the European Space Research and Technology Centre, European Space Agency, Noordwijk, The Netherlands, for two months. In 2018, he was a Visiting Professor with the Edward S. Rogers Sr. Department of Electrical and Computer Engineering, University of Toronto, Toronto, ON, Canada. In 2019, he was a Visiting Professor with the Institute of Sensors, Signals and Systems, Heriot-Watt University, Edinburgh, U.K. His current research interests include the development of efficient analysis, design, and optimization techniques of reflectarray and transtmitarray antennas both in near- and far-fields.

Dr. Arrebola was a co-recipient of the 2007 S. A. Schelkunoff Transactions Prize Paper Award by the IEEE Antennas and Propagation Society.

MARCOS R. PINO was born in Vigo, Spain, in 1972. He received the M.Sc. and Ph.D. degrees in telecommunication engineering from the University of Vigo, Vigo, in 1997 and 2000, respectively.

In 1998, he was a Visiting Scholar with the ElectroScience Laboratory, The Ohio State University, Columbus, OH, USA. From 2000 to 2001, he was an Assistant Professor with the University of Vigo. Since 2001, he has been with the Department of Electrical Engineering, University of Oviedo at Gijón, Gijón, Spain, where he is currently an Associate Professor, teaching courses on communication systems and antenna design. From 2017 to 2019, he spent several months as a Visiting Fellow with the Department of Information Engineering, University of Pisa, Italy. His current research interests include antenna design, measurement techniques, and efficient computational techniques applied to EM problems, such as evaluation of radar cross section or scattering from rough surfaces.